Available online at www.sciencedirect.com

jmr&t Journal of Materials Research and Technology

journal homepage: www.elsevier.com/locate/jmrt

Original Article

On the short-time thermal phase-stability of as-cast $AlCoCrFeNi_{2.1}$ eutectic high entropy alloy

J. Charkhchian [a], *A. Zarei-Hanzaki* [a,**], *A. Moshiri* [a], *H.R. Abedi* [b,*], *Jiajia Shen* [c], *J.P. Oliveira* [c,d], *Kanwal Chadha* [e], *Clodualdo Aranas Jr.* [e]

[a] *Hot Deformation and Thermomechanical Processing Laboratory of High Performance Engineering Materials, School of Metallurgy and Materials Engineering, College of Engineering, University of Tehran, Tehran, Iran*
[b] *School of Metallurgy & Materials Engineering, Iran University of Science and Technology (IUST), Tehran, Iran*
[c] *UNIDEMI, Department of Mechanical and Industrial Engineering, NOVA School of Science and Technology, Universidade NOVA de Lisboa, 2829-516 Caparica, Portugal*
[d] *CENIMAT/I3N, Department of Materials Science, NOVA School of Science and Technology, Universidade NOVA de Lisboa, 2829-516 Caparica, Portugal*
[e] *Mechanical Engineering, University of New Brunswick, Fredericton, NB E3B 5A3, Canada*

ARTICLE INFO

Article history:
Received 28 April 2022
Accepted 10 July 2022
Available online 20 July 2022

Keywords:
Eutectic high entropy alloy
Heat treatment
Ordered phase
Phase stability
Thermal stability

ABSTRACT

The present work deals with the short-time thermal phase-stability of the as-cast eutectic $AlCoCrFeNi_{2.1}$ high entropy alloy. Toward this end, the effect of different temperatures (800–1000 °C) and soaking times (15–60 min) on the stability of primary dendritic regions and formation of the ordered phases was explored. Microstructural characterization was supported by thermodynamic calculations and assessment of the subsequent mechanical properties. Upon the increase in annealing temperature and soaking time, the primary FCC dendritic areas grown and destabilized owing to elemental partitioning. This was followed by dendrite fragmentation and formation of needle shape B_2 ordered phases within the primary FCC regions. Despite the unstable nature of the primary constituent phases, the material hardness increased considerably to a peak point corresponding to the moderate soaking time of 45 min. The variation of the subsequent mechanical properties was discussed relying on the characteristics of the ordered and primary phases.

* Corresponding author.
** Corresponding author.
E-mail addresses: zareih@ut.ac.ir (A. Zarei-Hanzaki), habedi@iust.ac.ir (H.R. Abedi).

https://doi.org/10.1016/j.jmrt.2022.07.058

1. Introduction

High entropy alloys (HEAs) as a new emerging category of advanced materials, consist of five or more elements with an atomic percent ranging between 5% to 35% [1,2]. Among the various developed grades, the eutectic high entropy alloys (EHEAs) are of high interest, which owes the elimination of mushy zone (lack of solidification range), micro-segregation, and their excellent castability. Also, EHEAs have significantly tunable properties like (I) near-equilibrium microstructures resistance against changes at high-temperature servicing conditions (II) low-energy phase boundaries, (III) controllable microstructures (IV) regular lamellar or rod-like eutectic structures, and (V) capability to form an in-situ composite [3,4]. Such in-situ composite like structures, compared with conventional cast structures, include a soft face-centered cubic (FCC) phase and a hard body-centered cubic (BCC) phase provide acceptable combination of strength and ductility and excellent work hardening capacity [5,6].

The first EHEA with the composition of $AlCoCrFeNi_{2.1}$, which was developed by Lu et al. [7], had a lamellar microstructure including B_2 ordered phases and presented outstanding mechanical stability up to 700 °C. The thermal phase-stability of the same chemical composition was also investigated by Asoushe et al. [8]. It was shown that the volume fractions of FCC and BCC phases remained relatively unchanged during warm deformation up to 500 °C, which resulted in exceptional mechanical stability. Interestingly, the phase fraction of the as-cast microstructure after various thermomechanical processing such as cryo-rolling, warm rolling and hybrid-rolling was also found to be constant. Furthermore, the as-cast microstructure was developed into an heterogeneous one and an acceptable strength-ductility balance was achieved [9–11]. The previous research indicated that the as-cast microstructure of $AlCoCrFeNi_{2.1}$ EHEA through the hot-rolling and subsequent aging could achieve outstanding tensile properties, which is comparable with the cold-rolled microstructure due to the formation of B_2 precipitates during the long-term aging treatment [12]. The formation of the needle shape B_2 ordered phase during the heat treatment of EHEA was considered as a decisive concept in respect to thermal and mechanical stability. Accordingly, the mechanical behavior of the as-cast $Al_{0.6}CoFeNiCr_{0.4}$ was investigated after thermal treatment in the temperature range of 550–850 °C for 24 h, and demonstrated that the formation and evolution of ordered B_2 phase in the course of ageing improved the mechanical properties [13]. The earlier investigations on AlCoCrFeNi [14] and $Al_{0.6}CoCrFeNi$ [15] HEAs, revealed that the B_2 precipitates were formed during the aging process due to the transformation of $L1_2$ nano-precipitates to B_2 needle shape precipitates, which is triggered by the higher thermodynamic stability of B_2–NiAl precipitates. However, the previous research demonstrated that the formation of the needle shape B_2 phase in primary FCC can be observed through the long-term heat treatments at low-temperature range [16]. Interestingly, the strain induced precipitation of the B_2 phase was also reported by Zhang et al. [17] during hot-tensile deformation of $AlCoCrFeNi_{2.1}$ EHEA. In all cases, improvement in strength and hardness has been noted. Considering this fact that the presence of Aluminum (Al) and Nickel (Ni) in the chemical composition of the EHEA alloy provide a proper condition for the precipitation of ordered B_2 phase [18], and intensified elemental partitioning, the evolution of the FCC phase in the course of such short-time high-temperature annealing is highly probable. Despite the valuable efforts investigating the formation of the B_2 ordered phase, there is no systematic research exploring the effect of temperature and soaking time on the formation of the B_2 phase, especially at high-temperature regimes andas-cast microstructure. To bridge this gap, the present work has been steered towards the assessment of the thermal-phase-stability in $AlCoCrFeNi_{2.1}$ EHEA in the temperature/time range of 800–1000 °C and 15–60 min, to evaluate the evolution of FCC and B_2 ordered phases. Furthermore, the current work also explores the correlation between the mechanical properties and the probable microstructure evolutions during the aforementioned heat treatments.

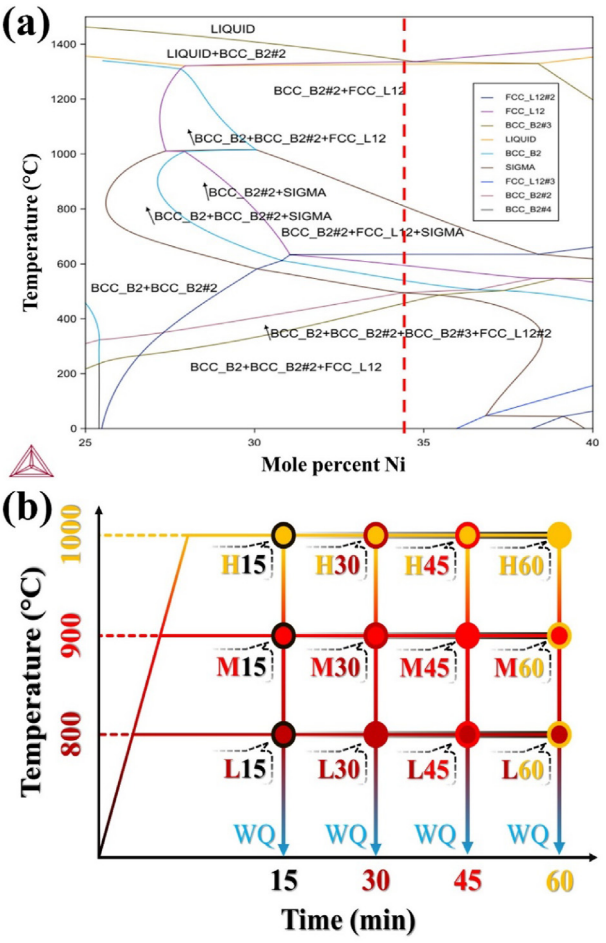

Fig. 1 – (a) Calculated equilibrium phase diagram as a function of Nickel content; the phase diagram was extracted from the ThermoCalc™ software, using the nominal composition of the $AlCoCrFeNi_{2.1}$ alloy, which is highlighted with a red dashed line. (b) Schematic view of the performed heat treatment procedures at different temperatures and soaking times.

2. Experimental procedures

The $AlCoCrFeNi_{2.1}$ EHEA with a nominal chemical composition of 16.4Al–16.4Co–16.4Cr–16.4Fe–34.4Ni (at%) was synthesized by vacuum induction melting. The ingot remelted at least 5 times to ensure good chemical homogeneity. To predict the equilibrium phases in the microstructure of the material, the equilibrium phase diagram has been constructed using ThermoCalc™ software (Fig. 1(a)). A dual phase FCC/BCC microstructure is stable from the melting point down to 750 °C, while the lower temperature can trigger the transformation of the primary FCC and BCC phases into new FCC and BCC phases [19]. In order to examine the phase stability of the primary duplex microstructure, the as-cast material was subjected to different heat treatments at different temperatures of 800, 900, and 1000 °C and different soaking times of 15, 30, 45, and 60 min. The corresponding heat treatment map is schematically illustrated in Fig. 1(b). The microstructures of the as-cast and heat-treated materials were characterized using optical microscope (OM, Meiji ML7100) and field emission scanning electron microscope (FE-SEM, KYKY EM8000), which was equipped with energy-dispersive X-ray spectroscopy (EDS) detector (Bruker, Xflash). X-ray diffraction (XRD, Rigaku Ultima IV) using Cu Kα radiation and a wavelength of 1.5406 Å was utilized to investigate the constituent phases in each microstructure. Electron backscatter diffraction (EBSD) analysis was also performed with the aid of a Thermo-Fisher Scientific/FEI's Scios 2 Dual-beam focused ion beam scanning electron microscopy (FIB-SEM) equipped with an integrated Oxford EBSD detector with 1000 nm step size. The hardness of the heat-treated microstructures was determined by the Vickers hardness (INNOVATEST hardness tester) test under a load of 2 kgf and a dwell time of 30 s. All of thermodynamic calculations were performed with the aid of the ThermoCalc™ software using the TCHEA4 database [20].

3. Results and discussions

The OM and SEM micrographs of the as-cast microstructure (Fig. 2(a) and (b)) demonstrate the primary simple FCC dendritic regions [21] separated by inter-dendritic areas, made up of ordered ($L1_2/B_2$) lamellar eutectic regions [22,23]. EDS point analysis was utilized to reveal the chemical composition of each constituent phase in the microstructure and the results have been listed in Fig. 2(b). The inter-dendritic regions is enriched with Ni and Al, which is attributed to the significantly low mixing enthalpy of Ni–Al couple (−22 kJ/mol) comparing with the other binary compounds in the experimented alloy [24]. For further clarification, the EBSD phase map analysis and X-ray pattern are depicted in Fig. 2(c) and (d), which confirm that the dual FCC/BCC with eutectic lamellar pattern of the starting microstructure.

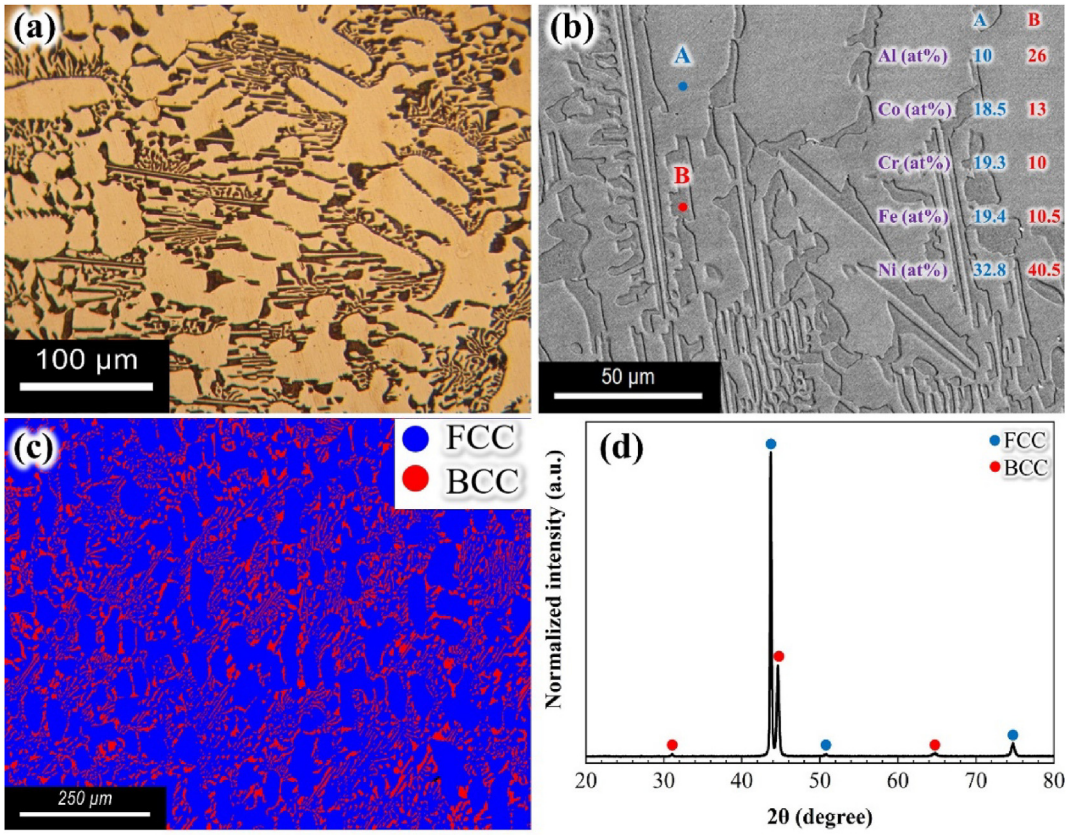

Fig. 2 – (a) The optical micrograph of as-cast initial microstructure; (b) the scanning electron microscopy (SEM) micrograph along with the corresponding energy-dispersive X-ray spectroscopy (EDS) point analysis of each phases; (c) electron backscatter diffraction (EBSD) phase map, and (d) the X-ray diffraction (XRD) pattern of the as-cast microstructure.

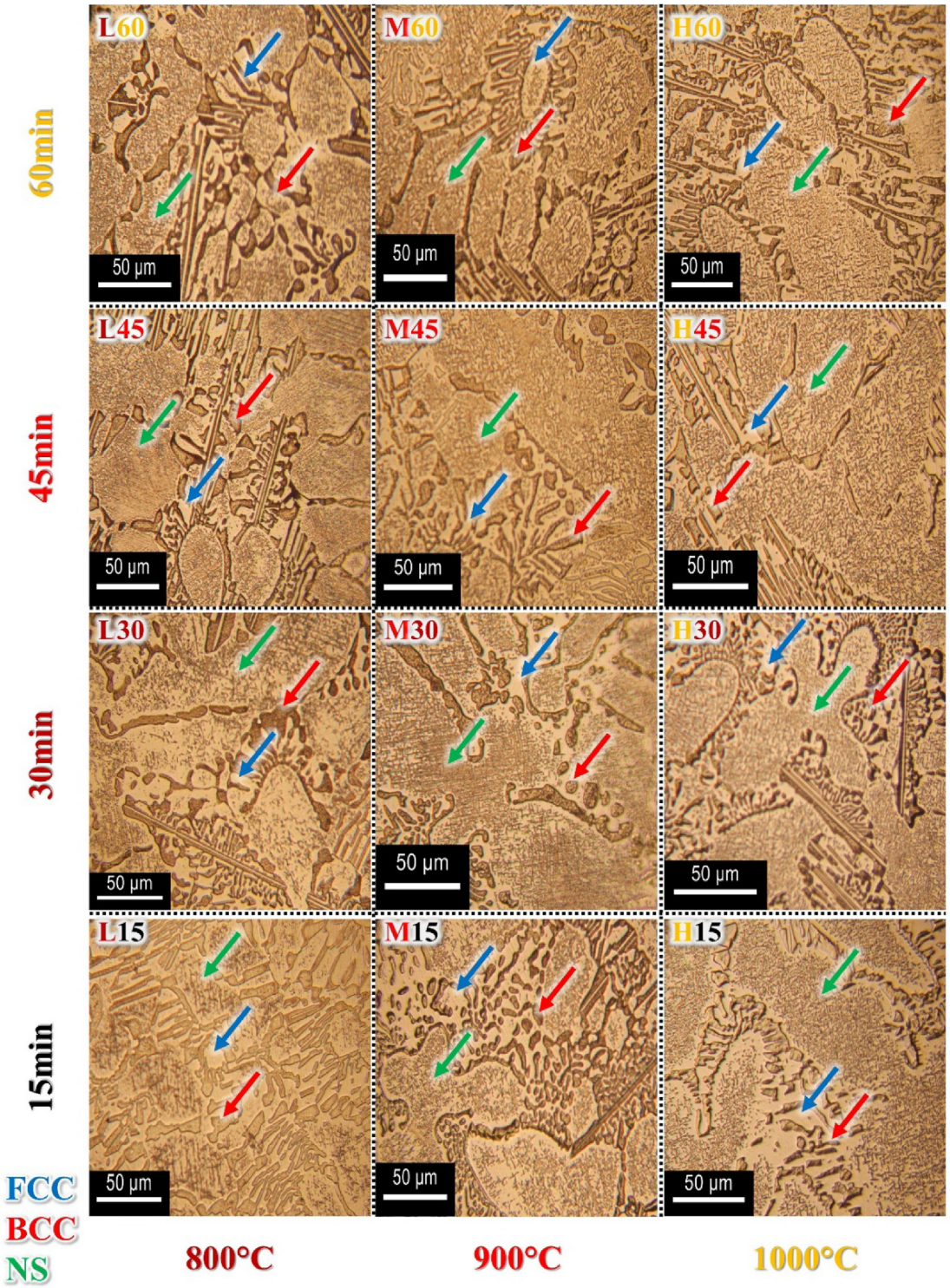

Fig. 3 – Optical micrographs of the heat-treated microstructures; blue, red, and green arrows correspond to the face-centered cubic (FCC), body-centered cubic (BCC), and the needle-shaped (NS) phases, respectively.

After executing the planned short-time heat treatments (Fig. 1(b)) on the as-cast material, the resulting microstructures were studied via OM, and the corresponding results have been depicted in Fig. 3. It is observed that in addition to the primary FCC and BCC phases (pointed out by blue and red arrows, respectively), fine needle-shaped (NS) precipitates were formed within the dendritic regions (marked by green arrows), which implies the instability of the FCC dendritic areas during the short-time annealing. Further analysis of the OM micrographs reveal that the annealing temperature and the soaking time have the same effect on the above-mentioned transformation; the higher temperature or time applied, the higher fraction of NS phases precipitate. A similar influence is evident on the primary dendritic region: raising the temperature as well as increasing the soaking time trigger these regions to coarsen and expand. However, comparing the OM images of the heat-treated microstructures for 45 and 60 min demonstrates that the expansion trend of FCC dendrites was ceased. This closely coincides with the observed variation in the fraction of needle-shape phase vs. annealing time (refer to Fig. 4). Furthermore, it is evident that the primary dendritic areas experienced considerable necking and fragmentation by increasing the annealing time, which is more intensified at higher temperatures. However, the NS phase formation, nature, and response to different heat treatments are still unclear and demand more accurate analysis via electron microscopy methods.

Figure 5 represents the SEM micrographs of the heat-treated microstructures at 800, 900, and 1000 °C for 15 min, respectively. It can be understood that primary FCC dendritic regions grew, and the transformed regions were increased. Furthermore, it can be realized from these results that as the temperature increased, the NS phase became coarser. Additionally, studying the elemental partitioning within the transformed regions of the heat-treated microstructures reveal the content of Ni and Al increased. Formation of similar Ni–Al rich needle-shaped phases with ordered B_2 structure in the FCC matrix has been also reported by Bönisch et al. [25]. The XRD patterns of the heat-treated microstructures at 800, 900, and 1000 °C for 15 min are shown in Fig. 6. Detailed examination demonstrates that increasing the peak intensity of the FCC phase at higher temperature (and increasing the fraction of B_2 phases) is accompanied with reduction of the BCC disorder phase fraction. This implies a complex elemental partitioning between FCC, BCC and ordered B_2 phase during annealing treatments.

Thermodynamic calculations were used to unveil the phases' thermal stability and calculate their corresponding Gibbs free energy. These results are exhibited in Fig. 7. The fraction of the FCC phase decreases with the decrease of temperature from the melting point, similar to the observed trends through experimental analysis. However, the FCC to BCC proportion from the thermodynamic point of view (Fig. 7(a)) (68/32) is completely different from the proportion characterized from microstructure analysis and X-ray diffraction in Fig. 2(c) and (d) (80/20). Considering the fact that the thermodynamic calculations is based on the equilibrium condition, and the aforementioned diffusional based mechanism is time dependent, the observed deviation seems to be reasonable. Also, the chemical potential energy of Al and Ni were plotted vs. temperature to interpret and predict the observed phase transformation in Fig. 7(c) and (d). Forasmuch as solid-state diffusion and elemental partitioning are triggered by a higher chemical potential energy to lower chemical potential energy and considering the fact that the chemical potential of Ni and Al in the FCC phase is higher than the ordered B_2 phase, the Al and Ni were clustered and formed the ordered B_2 precipitates (that enriched in Al and Ni) in the dendritic FCC regions.

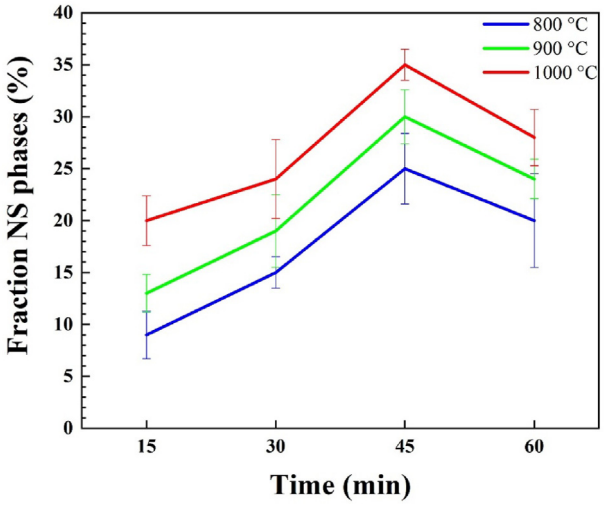

Fig. 4 – Variation of fraction of NS phases as a function of soaking time at different annealing temperatures.

Every boundary of the dendritic area acts as a surface defect increasing the energy of the dendrites [26]. Accordingly, the lesser surface-to-volume (S/V) ratio, a significant reduction in the energy level occurs. In the present study, raising the volume fraction of the dendritic regions by increasing the soaking time up to 45 min led to a considerable decrement in the S/V ratio, which resulted in more stability of the microstructure. Additionally, many researchers have proved that the curvature of these regions is another parameter that affects the area of the boundaries and therefore, the magnitude of surface energy; as the mean curvature increases, the surface energy reduces, which in turn triggers the spontaneous necking and fragmentation of the dendritic arms, which is known as Gibbs–Thomson effect [27–29]. This is considered the reason for the observed dendrite fragmentation in the present case (Fig. 8). Figure 7(b) which conveys that the Gibbs free energy of the FCC phase is significantly higher than that of the B_2 phase. Additionally, the fraction of FCC phase is remarkably higher than its equilibrium value, and the FCC phase is highly unstable. Considering all the above, the formation of B_2 NS phase can be attributed to the high driving force of the FCC to BCC transformation.

Figure 9 shows the Vickers hardness plots of the heat-treated samples, with focus on the effect of annealing temperature and soaking time on the resulting mechanical properties. According to the obtained data, increase of the heat

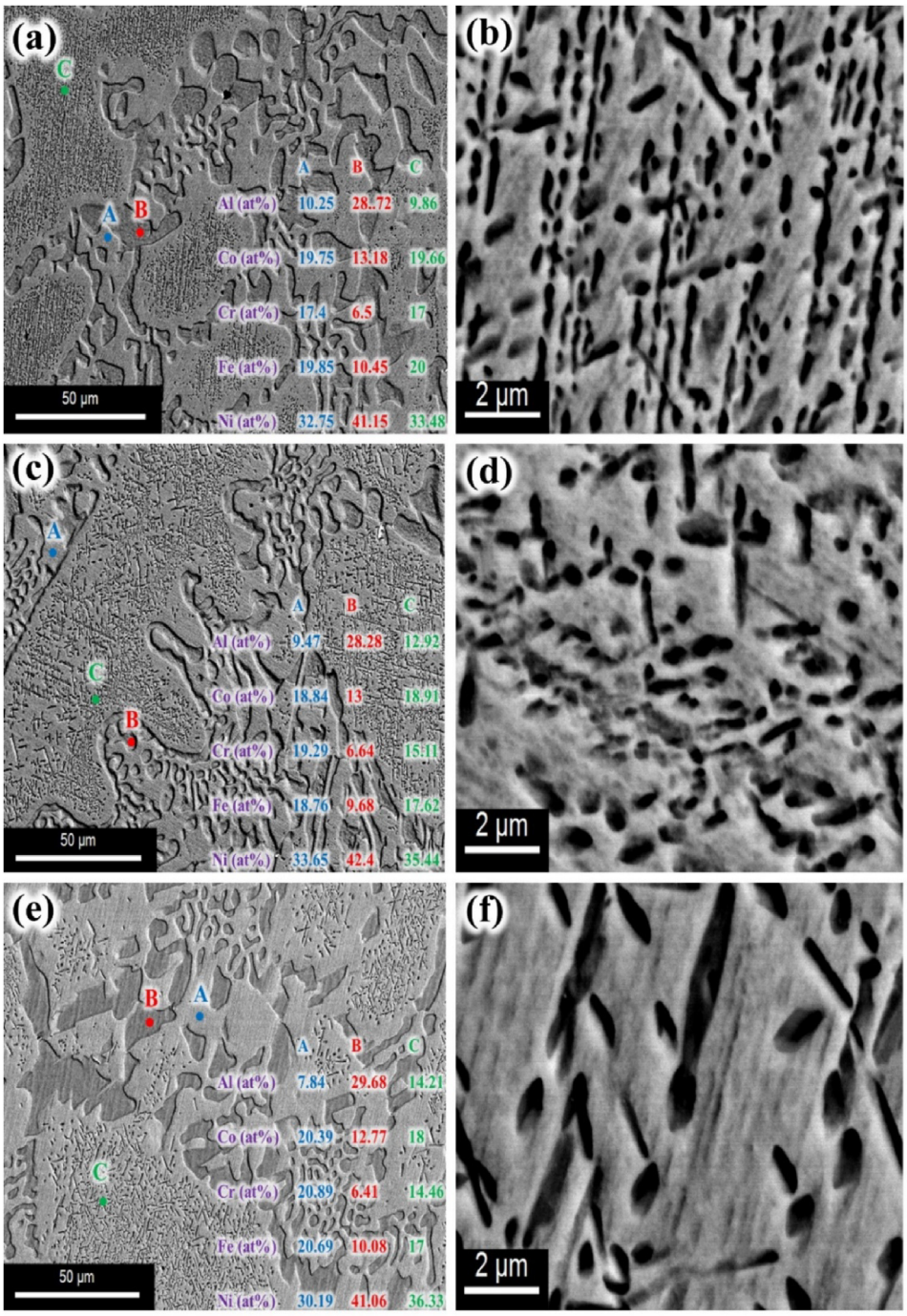

Fig. 5 – SEM micrographs and EDS point analysis results of the heat-treated microstructures at (a) 800, (c) 900, and (e) 1000 °C for 15 min; Blue, red, and green represent the FCC, BCC, and NS phase, respectively. (b), (d), (e) are the corresponding SEM close-ups of the NS phase at 800, 900, 1000 °C for 15 min respectively.

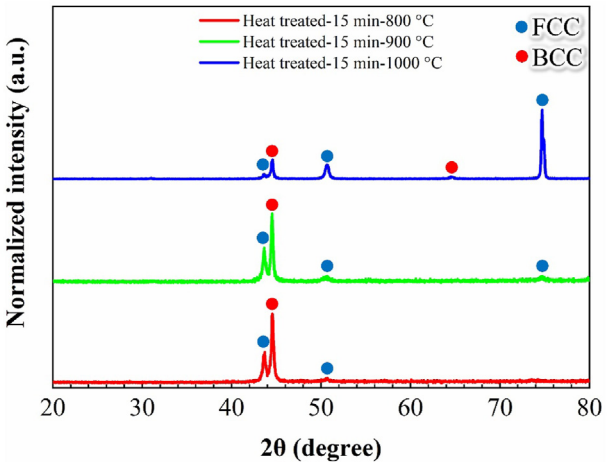

Fig. 6 – XRD patterns of the heat-treated microstructures at 800, 900, and 1000 °C for 15 min.

treatment time maximizes the hardness up to a peak of ~300 HV, followed by a gradually decreasing trend. It is generally accepted that coarsening of the precipitates make it harder for dislocations to move through the boundaries which in turn make the material harder [31]. Additionally, decreasing the frequency of the presence of precipitates reduce the probability of dislocation–precipitate interactions, which lead to lower hardness of the material [32]. As demonstrated in Fig. 3, the NS phases become more frequent in number up to 45 min in both 800 and 900 °C. Accordingly, the initial increment in the hardness-soaking time plot can be attributed to a considerable rise in the population of these precipitates in the FCC dendrite phases. Therefore, regarding the higher hardness of B_2 precipitates than the FCC matrix [30], the increment of the hardness value with increasing soaking time and annealing temperature, and acceleration of the formation of the B_2 NS phases in the higher time and temperatures, clearly demonstrate that the hardness values of the heat-treated specimens have a direct relationship with the aforementioned B_2 NS phase. Furthermore, it can be realized that adding more 15 min to the holding time at 800 and 900 °C stimulate the growth of these precipitates with lower quantity which in turn reduces the probability of dislocation–precipitate interactions and therefore lowers the magnitude of the material hardness. Comparing the micrographs of the samples obtained at 1000 °C with 800 and 900 °C (Fig. 3) it can be perceived that the coarsening procedure of the precipitates at 1000 °C triggers more rapidly than at lower temperature as a result of higher

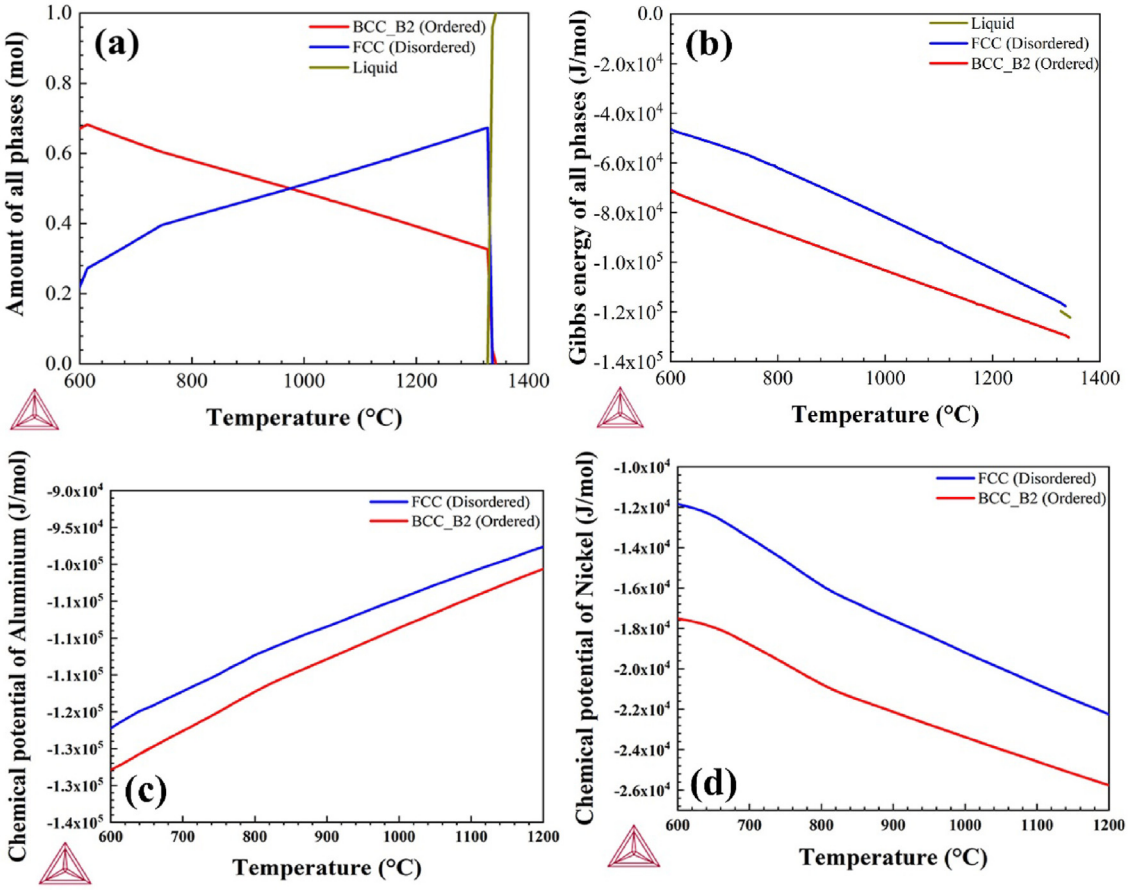

Fig. 7 – Theoretically (a) and (b) volume fraction of each phase and the Gibbs free energy as a function of temperature; (c) and (d) the chemical potential energy as a function of temperature for Aluminum and Nickel in the FCC and B_2 phases, which calculated using ThermoCalc™ software.

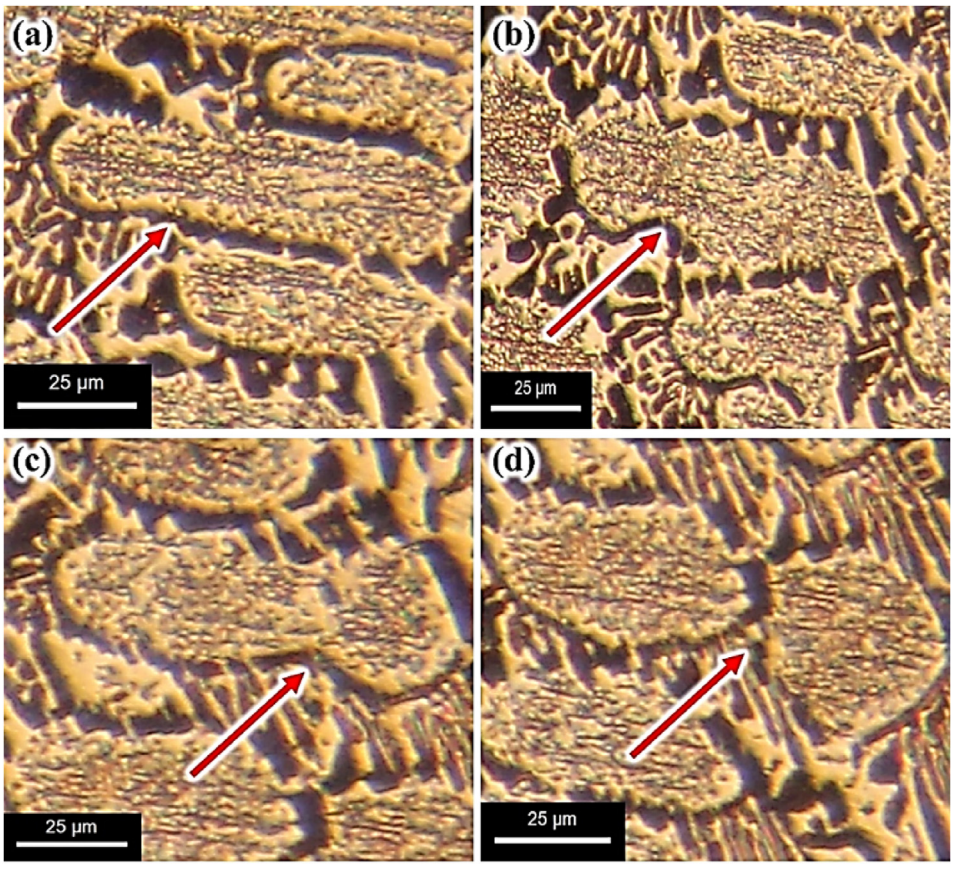

Fig. 8 – (a–d) Illustration of the sequence of the observed Gibbs–Thomson effect.

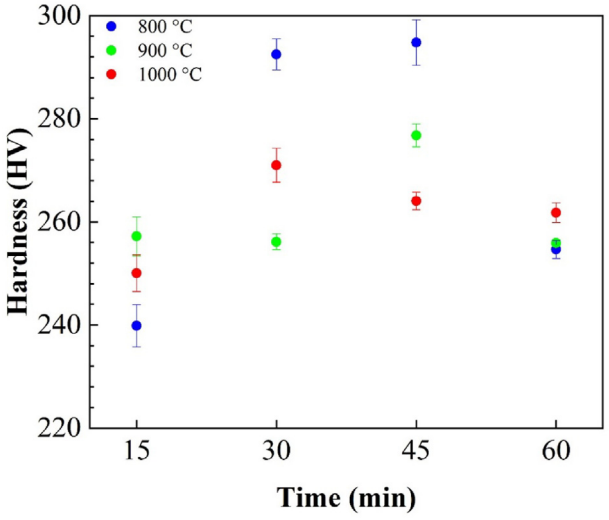

Fig. 9 – Average Vickers hardness of the heat-treated microstructures as a function of the applied temperature and soaking time.

diffusion rate in higher temperatures, which is also confirmed by the SEM images in Fig. 4. To this regard, the observed peak in the hardness-soaking time plot transfers into the lower times at higher temperatures.

4. Conclusions

In the current study, the effect of short-time heat treatments on the microstructural and hardness of $AlCoCrFeNi_{2.1}$ EHEA were investigated. The main findings can be summarized as follows:

- The primary FCC dendritic regions were found to be unstable in the course of short-time annealing at high temperatures, therefore the B_2 needle shape phase was formed within the unstable dendritic regions owing to the elemental partitioning.
- The Gibbs free energy of FCC phase was significantly higher than that of the B_2 phase. The FCC phase fraction was also higher rather than its equilibrium content. These stimulated the FCC to BCC transformation with increasing annealing temperature and soaking time.
- At the early stages of annealing the hardness increased as a function of soaking time, which was attributed to the formation of B_2 needle shaped precipitates and subsequent increase of their fraction. Further holding at high temperature led to coarsening of precipitates and decreased their frequency, which caused a gradual decrement in the hardening magnitude.

Declaration of Competing Interest

The authors declare that they have no known competing financial interests or personal relationships that could have appeared to influence the work reported in this paper.

Acknowledgments

The authors would like to gratefully acknowledge the kind support of Clodualdo Aranas, who the NSERC Discovery Grant supported by the Natural Sciences and Engineering Research Council of Canada (RGPIN 04006). Also, JPO acknowledges Fundação para a Ciência e a Tecnologia (FCT – MCTES) for its financial support via the project UID/00667/2020 (UNIDEMI). JPO also acknowledges the funding of CENIMAT/i3N by national funds through the FCT-Fundação para a Ciência e a Tecnologia, I.P., within the scope of Multiannual Financing of R&D Units, reference UIDB/50025/2020–2023. JS acknowledges the China Scholarship Council for funding the Ph.D. grant (CSC No. 201808320394).

REFERENCES

[1] Yeh JW, Chen SK, Lin SJ, Gan JY, Chin TS, Shun TT, et al. Nanostructured high-entropy alloys with multiple principal elements: novel alloy design concepts and outcomes. Adv Eng Mater 2004;6:299–303. https://doi.org/10.1002/adem.200300567.

[2] Cantor B, Chang ITH, Knight P, Vincent AJB. Microstructural development in equiatomic multicomponent alloys. Mater Sci Eng A 2004;375–377:213–8. https://doi.org/10.1016/j.msea.2003.10.257.

[3] Lu Y, Dong Y, Jiang H, Wang Z, Cao Z, Guo S, et al. Promising properties and future trend of eutectic high entropy alloys. Scr Mater 2020;187:202–9. https://doi.org/10.1016/j.scriptamat.2020.06.022.

[4] Gao X, Lu Y, Zhang B, Liang N, Wu G, Sha G, et al. Microstructural origins of high strength and high ductility in an AlCoCrFeNi2.1 eutectic high-entropy alloy. Acta Mater 2017;141:59–66. https://doi.org/10.1016/j.actamat.2017.07.041.

[5] Bhattacharjee T, Zheng R, Chong Y, Sheikh S, Guo S, Clark IT, et al. Effect of low temperature on tensile properties of AlCoCrFeNi2.1 eutectic high entropy alloy. Mater Chem Phys 2018;210:207–12. https://doi.org/10.1016/j.matchemphys.2017.06.023.

[6] Shi P, Ren W, Zheng T, Ren Z, Hou X, Peng J, et al. Enhanced strength–ductility synergy in ultrafine-grained eutectic high-entropy alloys by inheriting microstructural lamellae. Nat Commun 2019;10:1–8. https://doi.org/10.1038/s41467-019-08460-2.

[7] Lu Y, Dong Y, Guo S, Jiang L, Kang H, Wang T, et al. A promising new class of high-temperature alloys: eutectic high-entropy alloys. Sci Rep 2014;4:1–5. https://doi.org/10.1038/srep06200.

[8] Asoushe MH, Hanzaki AZ, Abedi HR, Mirshekari B, Wegener T, Sajadifar V, et al. Thermal stability , microstructure and texture evolution of thermomechanical processed AlCoCrFeNi 2.1 eutectic high entropy alloy. Mater Sci Eng, A 2021;799.

[9] Reddy SR, Yoshida S, Sunkari U, Lozinko A, Joseph J, Saha R, et al. Engineering heterogeneous microstructure by severe warm-rolling for enhancing strength-ductility synergy in eutectic high entropy alloys. Mater Sci Eng A 2019;764:138226. https://doi.org/10.1016/j.msea.2019.138226.

[10] Bhattacharjee T, Wani IS, Sheikh S, Clark IT, Okawa T, Guo S, et al. Simultaneous strength-ductility enhancement of a nano-lamellar AlCoCrFeNi2.1 eutectic high entropy alloy by cryo-rolling and annealing. Sci Rep 2018;8:1–8. https://doi.org/10.1038/s41598-018-21385-y.

[11] Reddy SR, Yoshida S, Bhattacharjee T, Sake N, Lozinko A, Guo S, et al. Nanostructuring with structural-compositional dual heterogeneities enhances strength-ductility synergy in eutectic high entropy alloy. Sci Rep 2019;9:1–9. https://doi.org/10.1038/s41598-019-47983-y.

[12] Liu Z, Xiong Z, Chen K, Cheng X. Large-size high-strength and high-ductility AlCoCrFeNi2.1 eutectic high-entropy alloy produced by hot-rolling and subsequent aging. Mater Lett 2022;315:131933. https://doi.org/10.1016/j.matlet.2022.131933.

[13] Wang S, Zhao Y, Xu X, Cheng P, Hou H. Evolution of mechanical properties and corrosion resistance of Al0.6CoFeNiCr0.4 high-entropy alloys at different heat treatment temperature. Mater Chem Phys 2020;244:122700. https://doi.org/10.1016/j.matchemphys.2020.122700.

[14] Nandal V, Harun B, Sarvesha R, Singh SS, Huang EW, Chang YJ, et al. Revealing the precipitation sequence with aging temperature in a non-equiatomic AlCoCrFeNi high entropy alloy. Metall Mater Trans A Phys Metall Mater Sci 2022;53:314–21. https://doi.org/10.1007/s11661-021-06528-7.

[15] Shang G, Zheng W, Wang J, Lu X-G. Microstructural evolution and local mechanical properties of dendrites in Al0.6CoCrFeNi high entropy alloy. Mater Sci Eng A 2022;846:143294. https://doi.org/10.1016/j.msea.2022.143294.

[16] Huang X, Dong Y, Lu S, Li C, Zhang Z. Effects of homogenized treatment on microstructure and mechanical properties of AlCoCrFeNi2.2 near-eutectic high-entropy alloy. Acta Metall Sin (Engl Lett) 2021;34:1079–86. https://doi.org/10.1007/s40195-021-01196-3.

[17] Zhang Y, Wang X, Li J, Huang Y, Lu Y, Sun X. Deformation mechanism during high-temperature tensile test in an eutectic high-entropy alloy AlCoCrFeNi2.1. Mater Sci Eng A 2018;724:148–55. https://doi.org/10.1016/j.msea.2018.03.078.

[18] Shukla S, Wang T, Cotton S, Mishra RS. Hierarchical microstructure for improved fatigue properties in a eutectic high entropy alloy. Scr Mater 2018;156:105–9. https://doi.org/10.1016/j.scriptamat.2018.07.022.

[19] Choudhuri D, Gwalani B, Gorsse S, Mikler CV, Ramanujan RV, Gibson MA, et al. Change in the primary solidification phase from fcc to bcc-based B2 in high entropy or complex concentrated alloys. Scr Mater 2017;127:186–90. https://doi.org/10.1016/j.scriptamat.2016.09.023.

[20] Software T. THERMO-CALC & DICTRA, computational tools for materials science J-O andersson, thomas Helander,Lars hdghmd, pingfang shi, bo sundman. Calphad Comput Coupling Phase Diagrams Thermochem 2002;26:273–312.

[21] Nassar A, Mullis A, Cochrane R, Aslam Z, Micklethwaite S, Cao L. Rapid solidification of AlCoCrFeNi2.1 high-entropy alloy. J Alloys Compd 2022;900:163350. https://doi.org/10.1016/j.jallcom.2021.163350.

[22] Wani IS, Bhattacharjee T, Sheikh S, Bhattacharjee PP, Guo S, Tsuji N. Tailoring nanostructures and mechanical properties of AlCoCrFeNi2.1 eutectic high entropy alloy using thermo-mechanical processing. Mater Sci Eng A 2016;675:99–109. https://doi.org/10.1016/j.msea.2016.08.048.

[23] Wani IS, Bhattacharjee T, Sheikh S, Lud YP, Chatterjee S, Bhattacharjeea PP, et al. Ultrafine-grained AlCoCrFeNi2.1

eutectic high-entropy alloy. Mater Res Lett 2016;4:174–9. https://doi.org/10.1080/21663831.2016.1160451.
[24] Takeuchi A, Inoue A. Classification of bulk metallic glasses by atomic size difference, heat of mixing and period of constituent elements and its application to characterization of the main alloying element. Mater Trans 2005;46:2817–29. https://doi.org/10.2320/matertrans.46.2817.
[25] Bönisch M, Wu Y, Sehitoglu H. Twinning-induced strain hardening in dual-phase FeCoCrNiAl0.5 at room and cryogenic temperature. Sci Rep 2018;8:1–10. https://doi.org/10.1038/s41598-018-28784-1.
[26] Porter David A, Kenneth E, Easterling MS. Phase transformations in metals and alloys, vol. 59; 1983. https://doi.org/10.1016/0025-5416(83)90095-2.
[27] Laplanche G. Growth kinetics of σ-phase precipitates and underlying diffusion processes in CrMnFeCoNi high-entropy alloys. Acta Mater 2020;199:193–208. https://doi.org/10.1016/j.actamat.2020.08.023.
[28] Bridges D, Xu R, Hu A. Microstructure and mechanical properties of Ni nanoparticle-bonded Inconel 718. Mater Des 2019;174:107784. https://doi.org/10.1016/j.matdes.2019.107784.
[29] Perez M. Gibbs–Thomson effects in phase transformations. Scr Mater 2005;52:709–12. https://doi.org/10.1016/j.scriptamat.2004.12.026.
[30] Yang T, Xia S, Liu S, Wang C, Liu S, Zhang Y, et al. Effects of AL addition on microstructure and mechanical properties of AlxCoCrFeNi High-entropy alloy. Mater Sci Eng A 2015;648:15–22. https://doi.org/10.1016/j.msea.2015.09.034.
[31] Shun T-T, Du Y-C. Age hardening of the Al0.3CoCrFeNiC0.1 high entropy alloy. J Alloys Compd 2009;478:269–72. https://doi.org/10.1016/j.jallcom.2008.12.014.
[32] Kafexhiu F, Podgornik B, Feizpour D. Tribological behavior of as-cast and aged AlCoCrFeNi2.1 CCA. Metals 2020;10. https://doi.org/10.3390/met10020208.

FURTHER READING

[1] Assadi H, Reutzel S, Herlach DM. Kinetics of solidification of B2 intermetallic phase in the Ni–Al system. Acta Mater 2006;54:2793–800. https://doi.org/10.1016/j.actamat.2006.02.018.